

# VALIDATION OF RANSE SIMULATIONS OF A FULLY APPENDED ACC V5 DESIGN USING TOWING TANK DATA

C. Böhm, R&D Centre Univ. Appl. Sciences Kiel, Yacht Research Unit, Germany

K. Graf, Univ. Applied Sciences Kiel, Germany

## SUMMARY

The paper presents results of free surface RANSE simulations of the flow around an ACC V5 Americas Cup yacht. The RANSE simulation is coupled with a method for the solution of the equation of motion to account for dynamic trim and sinkage. The paper discusses gridding methods and calculation setup. Results are compared with model tests of small scale factor. The paper shows that a small test matrix can be sufficient to generate hydrodynamic coefficients for VPP-integration. Computational run times are discussed as well as general turn around times. The paper finishes with a discussion of pros and cons of RANSE simulations versus towing tank testing.

## NOMENCLATURE

c	volume fraction	$\vec{u}_\infty$	undisturbed
CV	control volume	$\vec{u}_{per}$	perturbation velocity
$F_H$	heeling force	$\vec{u}$	vector of flow velocity
$F_X$	flow force in tank longitudinal direction	$VCE_{Aero}$	vertical distance of aerodynamic forces from force balance centre
$F_{z,DYN}$	dynamic sinkage force	$\alpha$	angle of attack
$F_z$	total vertical force component	$\varphi$	heel angle
$F_{z,Hydro}$	vertical component of the fluid force acting on the body	$\lambda$	scale factor
$\vec{F}_{Hydro}$	total fluid force acting on the body	$\delta$	rudder angle
$F_{z,Ext}$	vertical component of external forces	$\tau$	wall shear stress
g	acceleration of gravity	$\eta$	trim tab angle
$I_{yy}$	pitch moment of inertia	$\phi$	trim angle
J	mass moment of inertia	$\rho$	fluid density
k	turbulent kinetic energy	$\nu$	kinematic viscosity
L	Total length of the test case	$\nu_T$	turbulent viscosity
LCB	longitudinal centre of buoyancy	$\omega$	specific turbulence dissipation rate
LCG	longitudinal centre of gravity	$\Omega$	absolute value of vorticity
m	mass of the investigated body	$\mu$	molecular viscosity
$M_{y,DYN}$	Dynamic trim moment		
$M_y$	total trim moment		
$M_{y,Hydro}$	trim moment from fluid forces acting on the body		
$\vec{M}_{Hydro}$	total moment from fluid forces acting on the body		
$M_{y,Ext}$	external trim moment		
$\vec{n}_i$	unit normal vector of the CV surface		
p	pressure		
RMS	root mean square		
$R_T$	total resistance non-lifting condition		
$R_I$	induced resistance		
$R_H$	added resistance due to heel		
$r_H$	$R_H/R_T$		
SF	Sideforce		
$S_i$	CV face area		
T	draft		
$T_E$	effective draft		
$t_E$	$T_E/T$		
U	ship speed		
$u_i$	local velocity component		
$u_1$	main flow direction		
$u_2$	transverval flow component		
$u_3$	vertical flow component		
$u_3^*$	vertical flow component in wing plane		

## 1. INTRODUCTION

RANSE flow simulations are widely used for the design and optimization of high performance sailing yachts. RANSE simulations are flow analysis methods based on the solution of the Reynolds Averaged Navier Stokes equation. Applied to sailing yacht hulls and appendages these methods provide results comparable to towing tank test results, with the asset that analysis of local flow phenomena is far easier than in the towing tank. In addition RANSE simulations avoid scaling effects, which usually harm accuracy of towing tank testing. However it is common understanding that validation of simulation results still is desirable and should be conducted wherever possible. This holds in particular for RANSE simulations with free surfaces, simulations, that take into account the generation of waves due to the air-water interface at the water surface.

Yacht Research Unit Kiel has carried out hydrodynamic RANSE flow simulations for the *BMW Oracle Racing America's Cup* campaign. A large number of design alternatives have been analysed in order to optimize the appendage set, namely the keel fin, the ballast bulbs and the wings. These investigations

included free surface simulation in order to study the impact of wave generation on the flow forces generated by the appendages.

As an integral part of this study RANSE simulations of flow around a benchmark hull with appendages have been compared with respective towing tank test results. This comparison allowed to fine-tune the gridding process and the simulation setup. This paper reports about this validation study.

## 2. THEORETICAL METHOD

A RANSE solver is used to calculate the flow around the investigated hull and appendage set. Descriptions of RANSE methods are widely available, see Ferziger [2] as the authors' favourite. The governing equations of RANSE methods will be sketched here only briefly.

RANSE solver use a volume based method to solve the time-averaged Navier-Stokes equations in a computational domain around the investigated body. The RANS equation evolves from time averaging mass and momentum conservation for a continuous flow. In the method used it is assumed that the Reynolds stress evolving from time averaging is modelled using the eddy viscosity hypothesis and two-equation turbulence models. Assuming incompressible flow this yields,

$$\frac{\partial u_i}{\partial t} + \frac{\partial(u_j u_i)}{\partial x_j} = -\frac{1}{\rho} \frac{\partial(p + 2/3 \rho k)}{\partial x_i} + \frac{\partial}{\partial x_j} \left( (\nu + \nu_T) \left( \frac{\partial u_i}{\partial x_j} + \frac{\partial u_j}{\partial x_i} \right) \right) + g_i \quad (1)$$

$$\frac{\partial u_i}{\partial x_i} = 0 \quad (2)$$

The turbulence model used in the presented approach is Menter *Shear Stress Transport* (SST) model. It calculates the turbulent viscosity  $\nu_T$  from the turbulent kinetic energy  $k$  and the specific turbulent dissipation  $\omega$ :

$$\nu_T = \frac{a_1 k}{\max(a_1 \omega, \Omega F_2)} \quad (3)$$

In the present case to different fluids (water and air) have to be taken into account in the simulation. Therefore an additional conservation equation has to be introduced to capture the free surface interface and its deformation due to the yachts wave pattern. Since this fluids are not expected to mix, a homogenous multiphase model based on a Volume-of-Fluid (VOF) approach is applied, which assumes that the two phases share a common velocity and pressure field. Effectively the method treats both phase in the computational domain as one fluid with variable properties. The additional transport equation is solved for the VOF-fraction  $c$  in every cell, with values between 0 and 1 indicating a cell

which is filled with both fluids. The free surface interface is assumed to be represented by a value of  $c=0.5$ .

$$\frac{\partial c}{\partial t} + u_i \frac{\partial c}{\partial x_i} = 0 \quad (4)$$

The density  $\rho$  and molecular viscosity  $\mu$  are calculated from volume fraction  $c$  and the fluid properties as shown below. If a cell is filled with both fluids, they are assumed to share the same velocity and pressure.

$$\rho = \rho_1 c + \rho_2 (1 - c) \quad (5)$$

$$\mu = \mu_1 c + \mu_2 (1 - c) \quad (6)$$

To take into account the effects of dynamic trim and sinkage forces acting on the yacht a body motion module is embedded into the global RANSE iteration. The equations of motion of the rigid body are implemented as a 2-Degree-of-Freedom (DOF) method, but may be easily extended to more DOF if required. The translation and rotation resulting from the forces acting on the body are determined by integrating the equation of linear and angular momentum. The equation of linear momentum may be written as:

$$m \ddot{x}_z = F_z \quad (7)$$

Here  $m$  stands for the mass of the investigated body and  $\ddot{x}_z$  is the vertical component of its absolute linear acceleration. The contributions of external and internal forces to the resulting vertical force  $F_z$  is listed below.

$$F_z = F_{z,Hydro} + mg + F_{z,Ext} \quad (8)$$

Here  $g$  denotes the gravity which is positive in downward direction and  $F_{z,Ext}$  may be any external vertical force applied. A typical example here is the vertical component of the sail force generated in upwind test cases. The flow force  $F_{z,Hydro}$  is the total vertical component of the flow field acting on the body. It is determined from the RANS equations by integrating viscous wall shear stresses and pressure field over the body's surfaces.

$$\vec{F}_{Hydro} = \sum (-p_i \vec{n}_i + \vec{\tau}_i) S_i \quad (9)$$

Here  $p_i$  stands for the pressure acting on the surface of a control volume whilst  $\vec{n}_i$  is the normal vector of the individual control volume face. The viscous stresses are denoted  $\vec{\tau}_i$  and the surface of the control volume face is  $S_i$ .

In general, the equation of the angular momentum may be written as follows:

$$J \dot{\phi} = M_y \quad (10)$$

with  $J$  being the mass moment of inertia of the investigated body,  $\phi$  the trim angle around the transversal axis in Cartesian coordinates, and  $M_y$  the pitch component of the total moment with respect to the coordinate origin.  $M_y$  is summarized as follows:

$$M_y = mg(LCB - LCG) + M_{y,Ext} + M_{y,Hydro} \quad (11)$$

Here  $mg(LCB - LCG)$  represents the trimming moment due to weight of the body.  $M_{y,Ext}$  is the torque induced from external forces, for example from sails which may be determined from flow code as  $M_{y,Ext} = F_x VCE_{Aero}$ . The dynamic contribution of the flow force to the trimming moment  $M_{y,Hydro}$  may be expressed via  $\vec{M}_{Hydro}$  as stated below.  $\vec{x}_i$  are the control volume face centre vectors.

$$\vec{M}_{Hydro} = \sum \vec{x}_i \times (-p_i \vec{n}_i + \vec{\tau}_i) S_i \quad (12)$$

The translation and rotation of the body is determined by integrating the equation of linear and angular momentum with an simple first order Euler approach which is modified for numerical stability. The resulting displacement and rotation angle are returned to the RANSE code. The single-grid strategy with a free moving body inside a fixed computational box which has been applied in this work requires a grid deformation algorithm. Here *CFX* intern grid morphing algorithm, which is based on a laplace approach, was used to deform the grid according to the flow forces. The body is rotated around its centre of buoyancy using the transformation of the position vector in a rotating coordinate system. Then the flow forces are updated and the resulting forces again used to solve the rigid body equation. This iterative procedure is carried out until convergence is achieved.

### 3. IMPLEMENTATION

The theoretical method as described in the previous chapter is implemented in the commercial RANSE code *Ansys CFX* 10/11, which has been used for the investigation presented here. *CFX* solves mass- and momentum transport equations using a finite volume approach with polyhedral grid cells, cartesian velocity components and a vertex based flow variable arrangement. For wall boundary conditions *CFX* uses scalable wall functions: an alternative formulation of the logarithmic wall function avoiding singularity for zero shear stress at separation locations. In addition the SST turbulence model uses a wall treatment scheme, where low Reynolds number modelling of turbulence is used near a wall if the local dimensionless wall distance  $y^+$  falls below the limits of the logarithmic wall functions.

To account for dynamic trim and sinkage a solution method for the equation of motion in 2 degrees of freedom is implemented, using *CFX Command*

*Language*. A simple forward Euler method is used to solve the ordinary differential equation of motion. An efficient relaxation scheme is used to accelerate convergence as described in detail in chapter 4.

*CFX* is fully parallelized using a domain decomposition approach and the SPMP (Single Program Multiple Data) approach to run on a network of individual machines. *PVM (Parallel Virtual Machine)* is used as the underlying messaging and synchronization mechanism.

At YRU-Kiel *CFX* runs on a 98-node Linux cluster. However due to stability reasons and for better parallel efficiency a typical parallel job allocates 30 processors, allowing to do a couple of runs in parallel. For the study presented here, a typical computational grid consists of approx. 4 million grid cells, resulting in 1.8 million computational polyhedral cells. A typical run time for an individual run on 30 processors is approx. 6 h to achieve a RMS residuum of  $10^{-4}$  for the transport equations and an imbalance of the vertical flow forces of less than 10 N.

### 4. TEST SETUP

The validation test case for the free surface calculation is the model M27, a towing tank model of a fully appended ACC V5 hull from the research program of *BMW Oracle Racing* for its challenge for the 32<sup>nd</sup> Americas Cup. Tank data of M27 has been available to the Yacht Research Unit Kiel.

For the purpose of validation of the simulation approach the M27 test case is investigated in the same model scale ( $\lambda=3$ ) used in towing tank testing. This is done to avoid errors due to model-to-full-scale transformation.

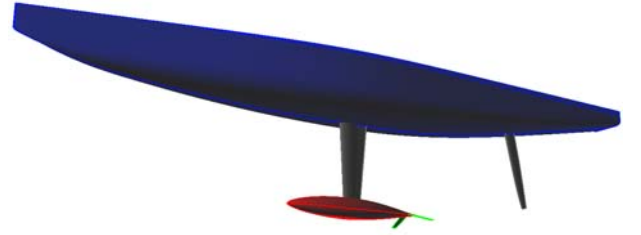


Figure 1: CAD-Model of the M27 test case

As a first step, the CAD-model of the fully appended hull is brought into an estimated static sailing trim by performing hydrostatics based on the yachts own weight and centre of gravity plus forces resulting from sails, crew and additional gear. The measurement weight of the full scale boat of 24t plus sail gear and crew weight result in a downwind sailing weight of 26.4t. This is corresponding to a displacement of the model of 953.02kg at  $\lambda=3$ .

The model is then mantled with an unstructured volume grid consisting of tetrahedral elements with prism refinements in both water plane and boundary layer area. It has to be noted here that *CFX*, the flow code used in the presented approach, modifies every

loaded grid into a polyhedral grid before performing flow calculation.

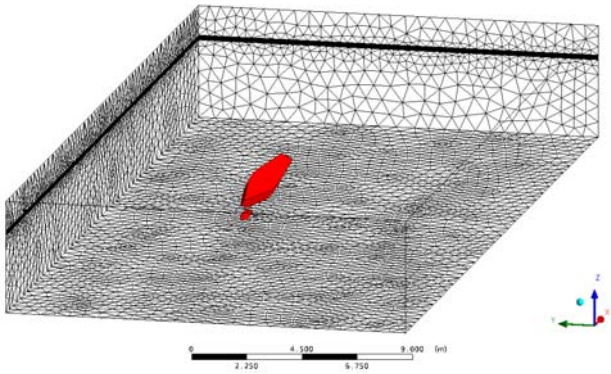


Figure 2: Computational Domain

The computational domain as shown in Figure 2 consists of approximately 4 million grid cells, including refinements in the expected area of the free surface and the boat surface. The grid spacing on the boat surfaces is shown in Figure 3.

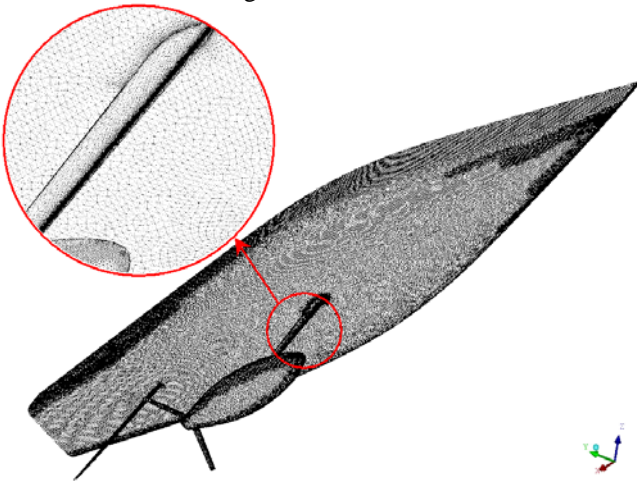


Figure 3: Surface grid applied on the testcase

The simulation environment around the M27 testcase extends  $1L$  to front and sides of the testcase and  $2.5L$  in the wakefield. The box extends  $0.5L$  above the hull and  $0.8L$  below. The box walls are treated as frictionless free slip walls whilst the M27 hull and appendages are treated as hydrodynamic smooth no-slip walls. At the Outlet a hydrostatic pressure in dependency to the location of the free surface is set. The inflow boundary conditions applied at the inlet are set depending on the test matrix as shown in Figure 9. The fluid properties are set to fresh water according to ITTC with a free stream turbulence intensity level of 2%.

To get realistic results, the effect of the dynamic sail forces acting on the hull have to be taken into account. Therefore additional trim moments and - in case of a lifting test case - sinkage forces have to be applied. For towing tank test these forces have to be estimated and applied prior to the testing which leads to some uncertainties. Normally during CFD calculations these forces may be determined and applied exactly as

derivations from resistance and sideforce. To enhance comparability between experiment and simulation the same trim moments and vertical forces applied in the towing tank were used for this validation.

With this settings the test setup is complete and the simulation may be started. After a start phase of about 100 iterations in which the initial flow field is allowed to consolidate, the body-motion module is called at every RANSE-iteration step and calculates the change in trim angle and sinkage due to the updated flow forces. According to these values the volume grid is deformed via CFXs grid morphing algorithm. The volume grid is only deformed in the near-field of the sailing yacht and outside of the boundary layer, thus making keeping the changes in the flow field to a minimum.

## 5. TOWINK TANK TESTS

### 5.1. RESISTANCE AND SIDE FORCE TESTS

Towing tank tests have been conducted by *BMW Oracle Racing* at the NRC-IOT towing tank in St.John's/Canada. Models of a scale factor  $\lambda=3$  have been used. They are equipped with studs as turbulence stimulators, located at a small distance from the stem/leading edge of the canoe body, fin, rudder, wings and bulb. Due to this turbulence stimulator locations fully turbulent flow can be assumed on the entire wetted surface. No resistance correction to account for turbulence stimulators' inherent resistance has been applied, assuming that drag reduction of the small laminar entrance zone balances the stimulator resistance.

For validation purposes test results of the model M27 have been available. M27 canoe body has been the model of the later US98, while appendages are used from an earlier design stage. The model has been tested at a sailing trim configuration conforming to a full scale total mass of approx. 26.4 t.

The following test matrix has been investigated:

- Resistance tests at non-lifting condition (no heel, no leeway, zero rudder and tab angle)
- Perturbation of heel angles of  $10^\circ$ ,  $20^\circ$ ,  $27.5^\circ$  and  $35^\circ$  with leeway angles of  $-1^\circ$ ,  $0^\circ$ ,  $1^\circ$  and  $2.5^\circ$ .
- For any combination of heel and leeway angle the boat velocity has been varied between 6kts. and 12 kts full scale.
- Rudder angle has been set to predefined values being constant for any combination of heel and leeway angle. No rudder sweep at constant values for heel and leeway has been carried out.

The entire test matrix consists of 117 test runs.

Processing of test results has been carried out according to [1]. For model to full-scale transformation of resistance at non-lifting condition the ITTC-78 performance prediction method has been used. Here Reynolds-number correction of viscous resistance has been done individually for the canoe body and the

appendage elements fin, rudder, bulb and wings. Figure 4 shows the drag area  $R_T / (0.5\rho U^2)$  over boat speed  $U$ .

For non-zero heel and leeway conditions the hydrodynamic properties of the yacht is described by the effective draft and the added resistance due to heel. Effective draft is defined as

$$T_E = \sqrt{\frac{F_H^2}{R_l 0.5\rho U^2 \pi}} \quad (13)$$

which can be derived from a leeway sweep at constant heel and boat speed by assuming:

$$\frac{R_l}{F_H^2} = \frac{dF_x}{d(F_H^2)} \quad (14)$$

Added resistance due to heel can be determined from the assumption that  $dF_x / d(F_H^2)$  is constant for a given combination of boat speed and heel angle. It is derived from a leeway sweep by a linear extrapolation of  $F_x = f(F_H^2)$  to zero heeling force  $F_H$ , giving the sum of upright resistance and added resistance due to heel.

Figure 5 shows the added resistance of M27, normalized with upright resistance, over boat speed and heeling angle. Figure 6 shows effective draft of M27, normalized with the geometric draft at sailing condition.

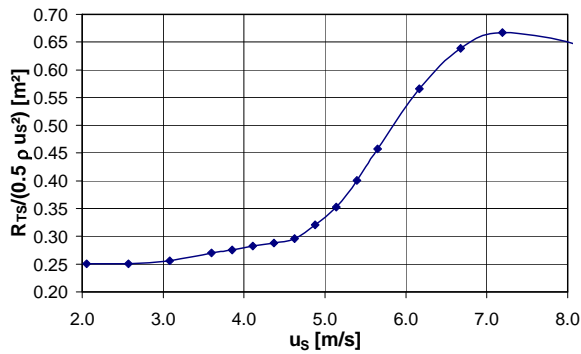


Figure 4: Resistance Area M27 at full scale

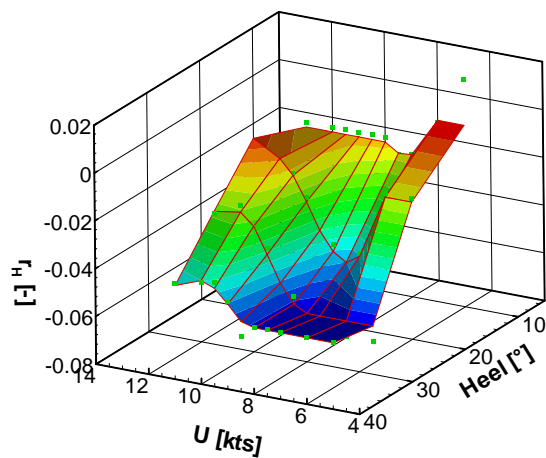


Figure 5: Coefficient of added resistance due to heel for model M27

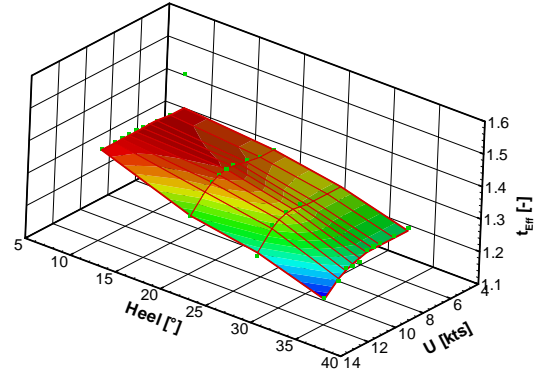


Figure 6: Effective draft coefficient M27

## 5.2. FLOW FIELD LDA MEASUREMENTS

Flow field measurement using a *Dantec Flow Light 2D* Laser Doppler Anemometer have been carried out in the open water circulation tank at YRU-Kiel. The objective of the study was to evaluate the impact of the free water surface on the incident flow of the keel wings. For these tests a small model of scale factor  $\lambda=17$  has been used. Wings have been removed for the measurements. Transverse and vertical flow velocity components have been measured in the sectional plane where the wings are located. A grid of approximately 1000 individual measurement points has been investigated. Figure 7 and Figure 8 show the LDA measurement system in action.

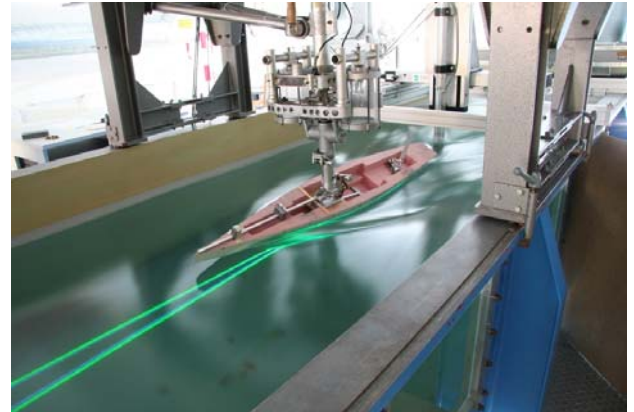


Figure 7: LDA in open water circulation tank



Figure 8: LDA measurements in wing sectional plane

Model investigations using a scale factor of  $\lambda=17$  provide only limited accuracy. However for a general proof of concept or a qualitative investigation the accuracy is quite sufficient. The advantage of model tests in an open water circulation tank is the ability to do a continuous test run at a constant velocity. This allows to acquire a large number of individual measurement samples of the flow field with limited resources. Doing flow field measurements of 1000 individual samples takes only some hours in a circulation tank while doing the same amount of measurement samples in a towing tank is probably practically not feasible.

## 6. RESULTS

In the following chapter the results of the validation of the computational method are shown. The validation consists of a velocity sweep in downwind and upwind sailing conditions and a additional yaw angle sweep for the upwind testcase. For details, see the test matrix (Figure 9).

### Test Matrix M27 Validation

#### Non-Lifting test conditions

$u$ ( $\lambda=1$ ) [kts]	$F_n$ [-]
8.0	0.307
9.0	0.345
10.0	0.384
11.0	0.422
12.0	0.461

#### Lifting Case - Yaw Sweep

			$u$ ( $\lambda=1$ ) [kts]		
$\varphi$ [°]	$\delta$ [°]	$\eta$ [°]	9	9.5	10
27.5	1.75	8		-1	
27.5	1.75	8	0	0	0
27.5	1.75	8		1	

Figure 9: Validation Test Matrix

The flow simulation model has been set up for sailing flotation as described in chapter 4. Additional sinkage forces and trim moments due to sail pressure have been taken into account according to the towing tank data.

In Figure 10 a plot of convergence history for a free floating upwind case of the ACC model travelling at the full scale equivalent of 10 knots is shown. At the start of the simulation the body is held fixed to get a preliminary solution. Then sinkage force and trim moment are released consecutively to avoid crosstalk which might result in numerical instabilities.

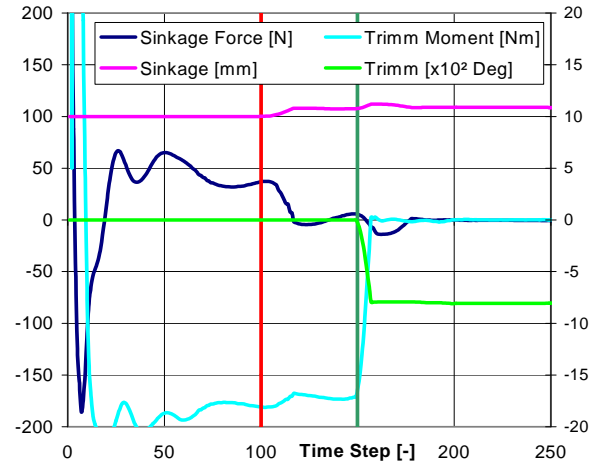


Figure 10: Convergence behaviour of sinkage force and trim moment

One can see from the time convergence plot, that after the yacht is released sinkage force (red mark) and trim moment (green mark) quickly converge towards equilibrium state. It can be generally stated that the remaining force and moment defects are small, being in the range of under 10 N respective Nm.

### 6.1. RESISTANCE

The resistance values obtained from simulations and towing tank tests for the M27 test case are shown in Figure 11 and Figure 13.

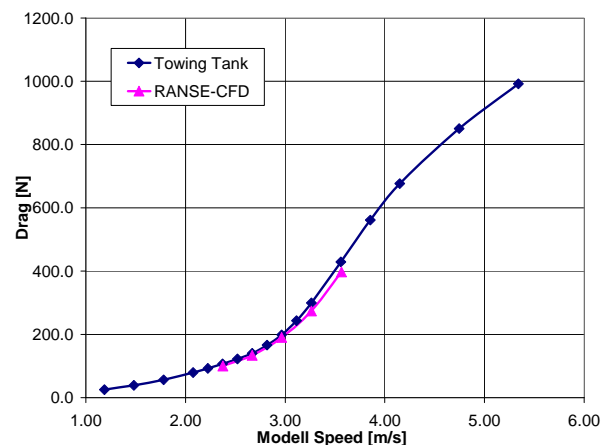


Figure 11: Comparison of resistance for the non-lifting testcase

Figure 11 depicts the resistance values of the non-lifting test case (downwind,  $\varphi=0^\circ$ ). The drag values obtained from the simulation are close to those of the tank tests but are also all smaller then those. Figure 12 shows the deltas between simulation and tank data for

resistance and sinkage. The deltas are calculated with respect to the towing tank data.

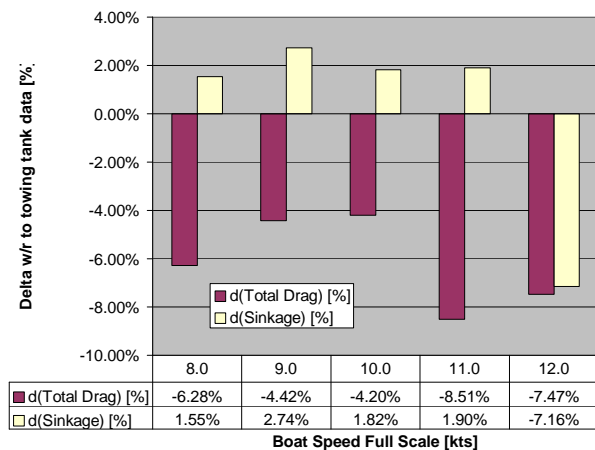


Figure 12: Deltas between measurement and simulation in downwind conditions

The differences for the resistance values rank from -4.5% for the lower model speeds to -8.5% for the higher speeds. The mean difference is a lower resistance of -6.2%. Differences for sinkage are quite evenly distributed around +2% with a peak at the highest boat velocity which is equivalent to 12 knots full scale.

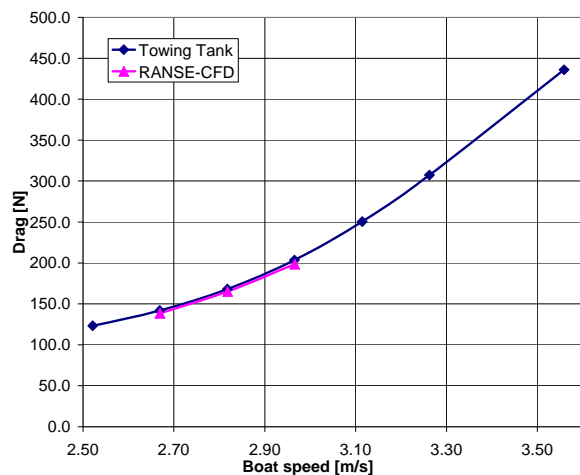


Figure 13: Comparison of drag upwind conditions

The next figure (Figure 13) shows the results for the upwind runs. These test cases are lift-generating since the M27 hull is heeled at  $\varphi=27.5^\circ$  and rudder and tab have been laid to  $\delta=1.75^\circ$  bzw.  $\eta=8^\circ$ . The yawing angle for these cases has been kept at  $0^\circ$ .

The trend obtained from these calculations is quite similar to that of the downwind test case with the simulated drag always being a bit lower than the measured drag. Figure 14 depicts the deltas of the simulation to the measurement for the upwind case. In addition to resistance and sinkage the deltas in sideforce are also shown.

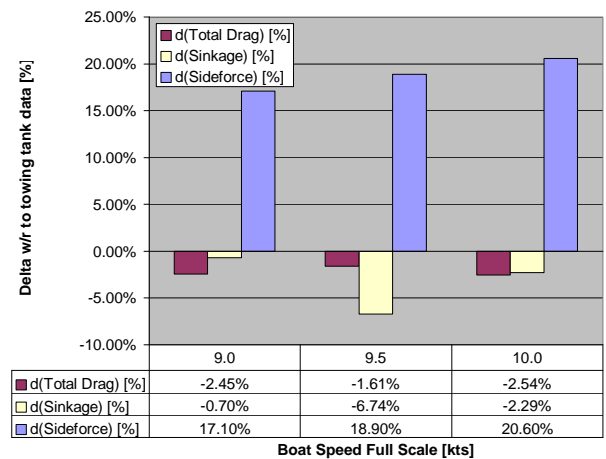


Figure 14: Deltas between measurement and simulation in lifting conditions

The difference between upwind and downwind results is that the drag deltas between tank test and simulation are smaller upwind. Here  $dF_x$  is ranging from -2.54% to -1.6% with the mean delta being -2.2%. Upwind the deltas in sinkage are scattering more than for the downwind case, but the more serious differences are the sideforce deltas which will be discussed in detail in 6.2.

The phenomenon of an underprediction of drag with a RANSE simulation is quite unusual. From theory one would expect that the drag values, especially the pressure drag, decrease with finer grid spacing until the point of grid invariance to the solution is met.

One possible error source could be a miss measurement of the drag measured in the towing tank. Since additional drag from turbulence stimulators should rise constantly with increasing Froude Number and this is not observed here, this source can be neglected. Other possible error sources are additional resistance due to confined water effects, but given the dimensions of the testing facility this seems rather unlikely.

As stated above, the towing tank does not seem to be a likely error source; therefore one should take a look at other uncertainties in this validations. From the simulation side there are several uncertainties which are located around the application of the dynamic sail loads.

- Applied Trim Moments and Vertical Forces as well as resulting trim angles and sinkage arose some questions which could not be clarified.
- The centre of efficiency of the trim moment assumed in the towing tank is unknown to YRU-Kiel.

These uncertainties may affect the trim of the hull in a way that the simulation leads to smaller resistance values. It is also possible that the wakefield hasn't been resolved fine enough. Here investigations with further refinements will be conducted, with first attempts looking rather promising, but the most likely error is a wrong trim due to the uncertainties mentioned above.

## 6.2. SIDE FORCES AND INDUCED RESISTANCE

Figure 15 and Figure 16 show the results of the yawing sweep which has been performed with the M27 testcase in upwind conditions. Yawing angles  $-1^\circ$ ,  $0^\circ$  and  $1^\circ$  have been tested at a model speed of 2.966m/s corresponding to a full scale speed of 9.5 knots.

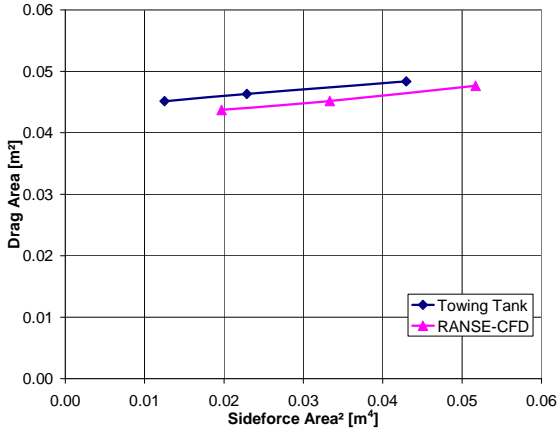


Figure 15: Drag Area over (SF Area)<sup>2</sup>

Figure 15 shows the results normalized as drag area over sideforce area squared, a presentation form which allows to draw conclusion about the effective draft of an appendage set. One could see that as in the prior results, the drag values of the simulation are also smaller here than those of the experiment. The sideforce, on the other hand seems to be heavily overestimated by the simulation. The differences in sideforce are ranging from +9.5% to +25%, the mean difference in  $d(SF)$  is 18.5%.

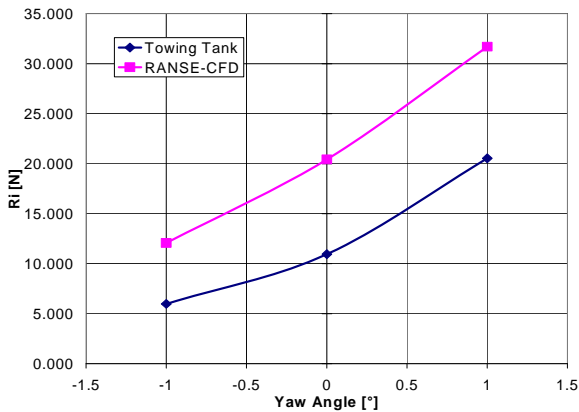


Figure 16: Comparison of Induced Resistance  $R_I$  between towing tank and CFD data.

A comparison of the induced resistance calculated from experiment and simulation is shown in Figure 16. Here the induced resistance of the simulation is quite a margin higher than that of towing tank test. This not surprising since the induced resistance  $R_I$  is a function of the heeling force which corresponds to the sideforce by

$$F_H = \frac{SF}{\cos \varphi} \quad (15)$$

One has to keep in mind, that determination of induced resistance is error-prone, since it is calculated from the difference of two large, almost equal values, since only the total resistance is predicted from experiments as well as from simulation.

Consequently a large overestimation of sideforce leads to an overestimated induced resistance. Such a large overestimation of sideforce by the simulation is quite unusual since RANSE methods are known to predict lift more accurate than drag. There are several possible error sources within the solution which are listed below.

A very likely source is the tab geometry, which was not exactly known for the simulation. An exact geometry should overcome this problem. There might also be some noise in the measurement data since exact measurement of such a high loaded, relative small fin is a hard task. Additionally the RANSE code is not taking into account the deflection of the blade. Another most likely error source is the trim problem with the reasons stated above for the resistance test.

Figure 17 and Figure 18 show some plots from the simulation

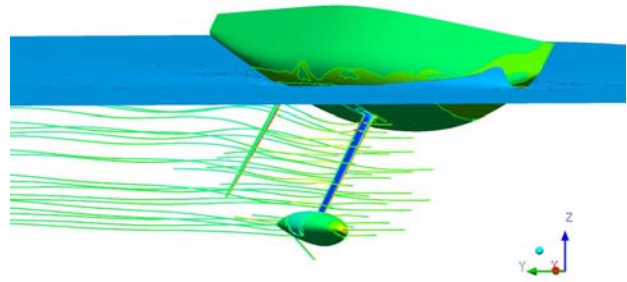


Figure 17: M27 test case travelling upwind at the equivalent of 10 knots

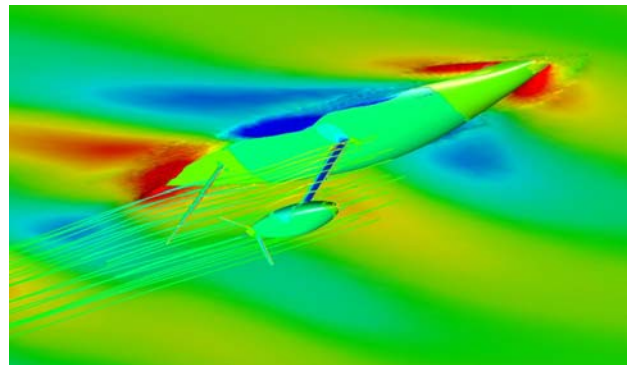


Figure 18: Free surface deformation around the M27 test case in upwind condition

## 6.3. LDA MEASUREMENTS

During appendage testing for ACC boats the question arose if the simplification of investigating the appendages released from the hull in a wind tunnel like environment is feasible. The alternative would be to test all appendage variants in a full free surface setup which would be very resource intensive, so an answer to this

question was rather important. An especially sensitive topic is the position and angle of attack of the wings, which have to be positioned very accurately to gain advantages from them. Small errors here will reduce efficiency of the wings or render them useless.

Therefore, measurements with a Laser Doppler Anemometer have been carried out to investigate the incidence flow the wings would experience with a free surface present. The same type of investigation has also been performed with RANSE free surface simulation to further confirm the results.

Figure 19 depicts the measurement raster for the lasers around the bulb. The raster indicates the measurement points per plane. The measurement have been undertaken with a 2D LDA from behind the yacht. The main advantage of LDA measurements is that the method comes without the need to introduce the measurement device directly into the area which has to be investigated.

To collect the data necessary for creating contour plots of the effective angle of attack  $\alpha$  in the area around the bulb, this raster has been scanned in several planes. The origin point of the reference system is chosen just behind the tab, marked by a red dot. Also Figure 19 shows the bulb with wings, these have been removed for the investigation to get the effective angle of attack the wings would experience without them acting on the flow field.

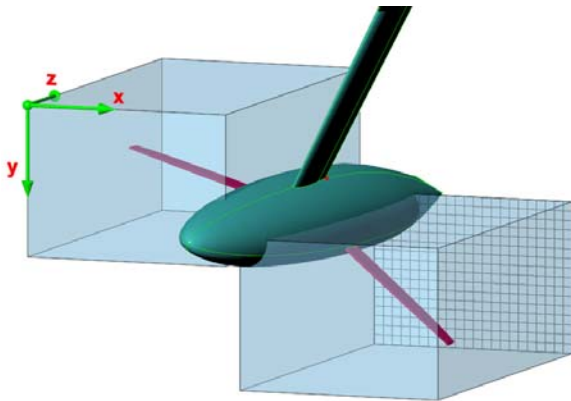


Figure 19: LDA-Measurement setup for the upwind case

To get the geometrical angle of attack (AoA) of the wings from the measurements for the upwind testcase, the velocity component  $u_3^*$ , which is acting vertical in the heeled boat plane, has been calculated from the vertical velocity  $u_3$  and the side velocity  $u_2$ .

$$u_3^* = u_3 \cos \varphi - u_2 \sin \varphi \quad (16)$$

Using the previously calculated velocity component  $u_3^*$  and the velocity of the main flow direction  $u_1$  one can obtain the angle of attack on the wings  $\alpha$ . For the experimental results it has to be mentioned that since the available LDA is operating in 2D mode, the velocity component  $u_1$  was not available. It is therefore considered that  $u_1$  is in first order similar to  $u_\infty$  which is measured in the circulation tank by an Ott-wing

$$\alpha = \arctan \left( \frac{u_3^*}{u_1} \right) \quad (17)$$

In the following some representative example results for both simulation and LDA measurement are displayed.

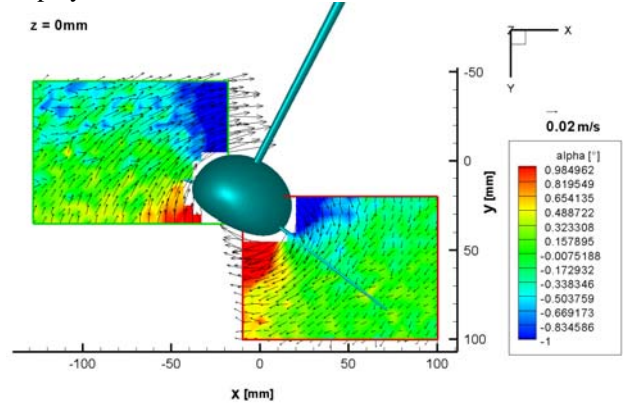


Figure 20: LDA - Measurement right behind the tab

Figure 20 shows the results from the LDA measurement at a position right behind the tab. The model has been tested at a model speed of 1.22m/s corresponding to a Froude Number of 0.38 ( $l=17$ ). Dynamic trim and sinkage have been taken into account. To resemble the original flow as near as possible the sideforce was brought to 3.5N (model scale). This sideforce corresponds to a tap angle of  $6^\circ$  and a rudder angle of  $-2^\circ$ .

One can see the vortex around the bulb as a result of the lift-generating keel blade. This vortex dominates the angle of attack of the wings so that no influence of the free surface is visible.

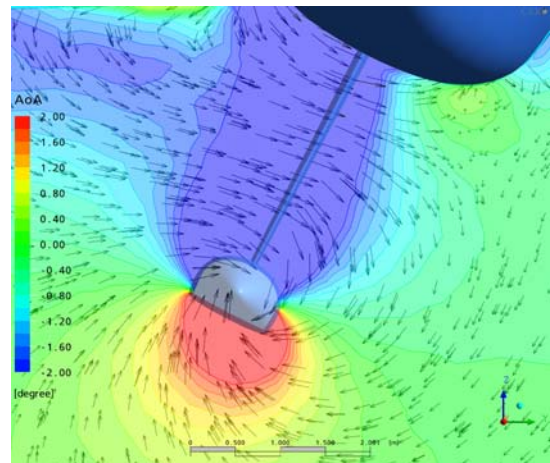


Figure 21: Cutting plane in simulation right behind tab

A typical result of the free surface simulation is shown in Figure 21 for a upwind case at  $\varphi=27.5^\circ$  and a boat speed of 10knots. The simulation has been performed in full scale to exclude effects coming a violation of Reynolds similarity.

The cutting plane shown in Figure 21 is at the same position as in the measurement (Figure 20). Here the contour plot shows the effective AoA in yacht-

coordinate system and the vector plot shows the perturbation velocity  $\vec{u}_{per}$  which is defined as  $\vec{u}_{per} = \vec{u} - \vec{u}_{\infty}$ . It has to be mentioned that the vectors have been normalized to uniform length so that the vector plot contains only direction information.

The findings of the simulation are quite similar to those obtained from the LDA measurements since they also shows that the dominant effect on the flow results from the displacement of the bulb and the vorticity induced by the lift generated from the blade. Compared with these effects the influence of the free surface on the flow field is negligible small.

From these results one can conclude that the assumption of considering the appendage set as deeply immersed is valid at least for a comparative study. Therefore wing optimization can be performed with the sole appendage set investigated in a wind tunnel like environment.

## 7. DISCUSSION

The paper presented here describes a validation study of free surface RANSE investigations of flow around a V5 America's Cup yacht. It was generally found, that the agreement of measurement and simulation results is satisfying to a high degree. While resistance under non-lifting conditions as well as induced resistance and added resistance due to heel shows good agreement of simulations and experiments, some more research has to be carried out to increase agreement for side forces.

As explained in chapter 6 the results bear some uncertainties regarding the correct trim and sinkage values from the towing tank. The trends obtained from the simulation with an underprediction of drag and an overprediction of lift clearly point into the direction that small differences in applied trimming moments and vertical forces between measurement and simulation are present. These uncertainties will hopefully be cleared out in the near future.

The investigation of effective incident flow on the winglets of the bulb show a good correlation between experiment and simulation. Here some uncertainties regarding the applicability of the common approach to test appendages, especially wings, uncoupled from the hull could be cleared out.

RANSE simulations provide a couple of advantages over tank tests. Towing tank test results have to be transformed to full scale. While the wave resistance and to a certain degree the viscous pressure drag can be obtained from towing tank tests, the frictional resistance is overpredicted, requiring some adjustments. This adjustment is usually done with a simple empirical formula for the frictional resistance coefficient. In contrast to this, RANSE simulations can be conducted at full scale Reynolds number, avoiding scale effects. No adjustment of frictional resistance is needed.

Testing of sailing yachts, may it be experimental or via simulation, require some dynamic trim moment and sink forces to account for respective loads due to sail forces. The dynamic trim moment is calculated from

$$M_{yDYN} = R_T VCE_{Aero} \quad (18)$$

while the dynamic sink force is calculated using

$$F_{zDYN} = F_H \cos \varphi \quad (19)$$

In the towing tank these moments and forces usually have to be estimated prior to testing and remain constant for a leeway sweep. In the iterative calculation loop of a RANSE-solver the dynamic moments and forces can be adapted to the actual resistance and heeling force. They vary with actual resistance and heeling force, thus resembling real physical correlations to a much higher degree. This increases the accuracy of the prediction, in particular in the case of a variational study of two designs, where the shape of the appendages changes significantly.

However the main advantage of RANSE investigations is its ability to allow studies of design alternatives with small variations of hull or appendage shape. These variational studies can be carried out using RANSE-solvers much more efficient than in the towing tank. Consequently the validation study presented here has been the starting point of a large investigation targeting the optimization of the *BMW Oracle Racing ACC* yacht appendages, which has been based on RANSE investigations to a quite high degree.

## 8. REFERENCES

1. GRAF, K. and BÖHM, C.: A New Velocity Prediction Method for Post-Processing of Towing Tank Test Results, Proc. 17th Chesapeake Sailing Yacht Symposium, Annapolis, Maryland, March 2005
2. FERZIGER, J.H. and PERIC, M.: Computational Methods for Fluid Dynamics, Springer, New York 2002
3. WHITE, F. M.: Viscous Fluid Flow, Mc-Hill Book Co, New York, 1991
4. ANSYS CFX INC.: ANSYS CFX-Solver Theory Guide, Canonsburg, 2006
5. ANSYS CFX INC.: ANSYS CFX-Solver Modelling Guide, Canonsburg, 2006

## 9. AUTHORS' BIOGRAPHIES

**Christoph Böhm** holds a diploma degree from the University of Applied Sciences Kiel. He is currently working as a flow scientist at the Yacht Research Unit Kiel. He is specialized on RANSE simulations of sailing yacht appendages and hulls as well as subsequent VPP integration.

**Kai Graf** is professor for ship hydrodynamics at the University of Applied Sciences Kiel and senior scientist of the Yacht Research Unit Kiel. Kai is working on sailing yacht aero- and hydrodynamics since 1998, being specialized on numerical simulation methods.